Terr. Atmos. Ocean. Sci., Vol. 19, No. 1-2, 83-92, April 2008 doi: 10.3319/TAO.2008.19.1-2.83(SA)

Gravity Anomaly and Satellite Altimetry in the China Seas: Applications to Geodynamics

Xiaotao Chang[1, 2, *], Chuanyin Zhang[1], Hanjiang Wen[1], and Jiancheng Li[3]

[1] *Chinese Academy of Surveying and Mapping, Beijing, 100039, China*
[2] *Key laboratory of Dynamical Geodesy, Chinese Academy of Sciences, Wuhan, 430077, China*
[3] *School of Geomatics, Wuhan University, Wuhan, 430079, China*

Received 15 November 2006, accepted 5 September 2007

ABSTRACT

Satellite altimetry has become an operational remote sensing technique with important applications to geodynamics. In the present paper, ocean floor topography and tectonic detection in the deep earth are investigated using gravity anomalies from global gravity models and satellite altimetry corrected for waveform distortions. We compute the spherical harmonic degree components of the gravity anomaly from gravity models (up to degree 360), and use inverse the Vening Meinesz formula in the remove-restore procedure to obtain the residual gravity anomaly components higher than degree 360. This paper is intended to give a geodynamical analysis on the gravity anomaly components from the crust, upper mantle, and lower mantle. On this base, the geodynamics background and mechanism in an area of the China Seas (25°N ~ 42°N, 118°E ~ 130°E) are studied. The evidence shows gravity anomaly of different degree in the study area is mainly due to mass distribution of different depth, and the dynamical imbalance from the geopotential imbalance should be responsible for global dynamics activities, which change the lithosphere structure through mantle circulation.

Key words: Satellite altimetry, Gravity anomaly, Geology, Geodynamics

Citation: Chang, X., C. Zhang, H. Wen, and J. Li, 2008: Gravity anomaly and satellite altimetry in the China Seas: Applications to geodynamics. Terr. Atmos. Ocean. Sci., 19, 83-92, doi: 10.3319/TAO.2008.19.1-2.83(SA)

1. INTRODUCTION

Over the last few decades satellite altimetry has developed into an operational space technique with very important applications to geodynamics. Altimetry-derived gravity is getting more and more useful for the research of geodynamics with its dense geographical distribution and high precision (Bosch 2004). In this paper, methods to estimate high precision gravity anomaly are studied, and together with geophysical data and gravity field models, they are employed in the detection of oceanic geological and geodynamical characteristics.

Satellite altimetry has earlier been recognized as a source of information that can provide valuable geophysical and geodynamical information for the inversion of altimetry-derived gravity anomaly. The relevant theory and methods have reached maturity to some extent. In some early studies, Dixon et al. (1983) estimated ocean depth from satellite observation, and Sandwell (1984) detected 72 seamounts never known in the southwest Pacific Ocean according to sea surface data analysis on the deflection of the vertical (DOV); see also Wessel and Smith (1995), Wessel and Lyons (1997). As an important study on the structure of the ocean crust, Hwang (1997) built the ocean depth model of the South China Sea according to satellite observation and sounding data.

In the application of high resolution high precision gravity anomaly, strong correlations have been found between the gravity anomaly and geological and geodynamical characteristics. Geophysical observations in an oceanic area, such as earthquake waves and magnetic anomaly detection will be helpful for the establishment of such correlations. For example, Turcotte et al. (1978) and David (1984) modeled the flexibility of the lithosphere from the ocean gravity anomaly and geoid anomaly.

In this paper, after the high precision gravity anomaly is obtained, we analyze the relationship between the gravity

* *Corresponding author*
E-mail: changtao@casm.ac.cn

anomaly and its correction items and compute the degree components of the gravity anomaly. The effect of ocean floor in the gravity anomaly is calculated and its distribution in the full resolution gravity anomaly spectrum is detected in the paper. On this basis, the lower mantle, upper mantle, and crustal components of the full resolution gravity anomaly spectrum are analyzed, and the geodynamics background and mechanism in the study area (defined as an area covering 25°N ~ 42°N, 118°E ~ 130°E) of the China Seas are investigated.

2. GRAVITY ANOMALY FROM SATELLITE ALTIMETRY

For better gravity anomaly recovery, waveform retracking is implemented to correct the altimeter range measurement in our study. Altimetry data used in our study is waveforms of phase E and phase F missions of ERS-1/GM observations and Geosat GM observations. Our waveform retracking method considers the characteristics of the waveform to detect the potential sub-waveforms according to different threshold levels to calculate the possible ranges responding to each leading edge, and then uses the geophysical corrections from the GDR (Geophysical data record) data to obtain possible sea surface heights, thereby determining the best possible sea surface height according to the introduced reference sea surface height (Guo et al. 2006). In order to see the effect of waveform retracking, we have compared the waveform retracking corrected data-derived and the GDR data-derived gravity anomaly with ship-borne gravity anomalies. The results show waveform retracking can improve gravity anomaly recovery by 16.3% (Chang et al. 2006).

In our research, an inverse Vening Meinesz formula is used to recover the gravity anomaly from the retracked satellite altimetry observation. In this method, DOV is first computed according to the sea surface observation, and then inverse Vening Meinesz formula is employed to compute the gravity anomaly.

FFT algorithms of the inverse Vening Meinesz formula fall into two classes: 1-D FFT (1 dimension fast Fourier transform) algorithm and 2-D FFT (1 dimension fast Fourier transform) algorithm (Haagmans et al. 1993). The inverse Vening Meinesz formula must be written as a convolution for both algorithms. The 2-D FFT algorithm is faster than, but not as precise as the 1-D FFT algorithm, because the latitudes of each parallel are approximately computed according to the mean latitude in the convolution function. The 1-D FFT algorithm is a combination of common integration and the FFT algorithm lying between common integration and the 2-D FFT algorithm, which integrates on the parallels by the FFT algorithm, then calculates the common integral of different parallels. So in the 1-D FFT algorithm, all gravity anomalies on a parallel are computed at one time, and the anomalies on different parallels are computed respectively (Schwarz et al. 1990).

Gravity anomaly Δg is defined in the Inverse Vening Meinesz as:

$$\Delta g = \frac{\gamma}{4\pi R}\iint_{\sigma}(3\csc\psi - \csc\psi\csc\frac{\psi}{2} - \tan\frac{\psi}{2})\frac{\partial N}{\partial\psi}d\sigma \qquad (1)$$

where ψ is a spherical distance from computation gpoint to moving point (i.e., the field angular distance with respect to the origin), σ unit sphere, γ normal gravity, R earth's mean radius, $1/R \cdot \partial N/\partial\psi$ DOV component in direction ψ. ψ and $1/R \cdot \partial N/\partial\psi$ are expressed as:

$$\sin\frac{\psi}{2} = [\sin^2\frac{1}{2}(\varphi_p - \varphi) + \sin^2\frac{1}{2}(\lambda_p - \lambda)\cos\varphi_p\cos\varphi]^{\frac{1}{2}} \qquad (2)$$

$$\frac{1}{R}\cdot\frac{\partial N}{\partial\psi} = \xi\cos\alpha + \eta\sin\alpha \qquad (3)$$

where ξ and η are north-south and west-east components of along-track DOV respectively, α azimuth between the computation point and the moving point, φ_p the latitude at point p.

In the FFT algorithm of inverse Vening Meinesz formula, we used the formula derived by Hwang (1998). It can be written as,

$$\Delta g(\lambda_p) = \frac{\gamma\Delta\lambda\Delta\varphi}{4\pi}F_1^{-1}\{\sum_{\varphi=\varphi_{\min}}^{\varphi\max}\{F_1[H'(\Delta\lambda_{qp})\cos\alpha_{qp}]\}F_1(\xi_{\cos}) + \{F_1[H'(\Delta\lambda_{qp})\sin\alpha_{qp}]\}F_1(\eta_{\cos})\} \qquad (4)$$

where the kernel function H' can be written as,

$$H' = -\frac{\cos\frac{\psi_{pq}}{2}}{2\sin^2\frac{\psi_{pq}}{2}} + \frac{\cos\frac{\psi_{pq}}{2}\left(3 + 2\sin\frac{\psi_{pq}}{2}\right)}{2\sin\frac{\psi_{pq}}{2}\left(1 + \sin\frac{\psi_{pq}}{2}\right)} \qquad (5)$$

The inverse Vening Meinesz formula gets singular in the innermost zone, where the distance between the computation point and the moving point is zero. We use formula derived by Chang et al. (2005) to estimate the innermost zone effect, and so to improve the precision of gravity anomaly recovery.

To estimate the gravity anomaly from ERS-1 and Geosat altimetry observation, we used GGM02C model (degree 2 - 180) (http://www.csr.utexas.edu/grace/gravity/ggm02) and EGM96 model (degree 181 - 360) (http://cddis.nasa.gov/926/egm96/egm96.html) in the remove-restore procedure. The obtained residual gravity anomaly is gravity anomaly components higher than degree 360 in full degree

gravity anomaly spectrum, and is used in the geological analysis in the study area of the China Seas. For the application to geological study, we have calculated the 2' × 2' grid value of the altimetry derived gravity anomaly in the study area (30°N ~ 40°N, 120°E ~ 125°E).

3. SPHERICAL HARMONIC COMPONENTS OF GRAVITY ANOMALY

The gravity potential W is the sum of the gravitational potential V and the potential Φ of the centrifugal force.

$$W = V + \Phi = V + \frac{1}{2}\omega^2(x^2 + y^2) \tag{6}$$

The gravitational potential V satisfies Laplace's differential equation in the space exterior to the ellipsoid and can be expanded into spherical harmonics as:

$$V = \frac{\mu}{r}\sum_{n=0}^{\infty}\sum_{m=o}^{n}\frac{a_e^n}{r^n}(\overline{C}_{nm}\cos m\lambda + \overline{S}_{nm}\sin m\lambda)\overline{P}_{nm}(\cos\theta) \tag{7}$$

where r, λ, θ are spherical coordinates, μ earth's gravitational constant, a_e the equatorial radius of the earth. $\overline{P}_{nm}(\cos\theta)$ is fully normalized harmonics, n and m are degree and order, $\overline{C}_{nm}, \overline{S}_{nm}$ are fully normalized harmonic coefficients:

$$P_{nm}(\cos\theta) = \frac{(1 - \cos^2\theta)^{\frac{m}{2}}}{2^n n!}\frac{d^{(n+m)}}{d(\cos\theta)^{(n+m)}}(\cos^2\theta - 1)^n \tag{8}$$

$$\overline{P}_{nm}(\cos\theta) = \sqrt{k(2n+1)\frac{(n-m)!}{(n+m)!}}\,P_{nm}(\cos\theta) \quad , \qquad k = \begin{cases} 1 \text{ for } m = 0 \\ 2 \text{ for } m \neq 0 \end{cases} \tag{9}$$

$$\begin{Bmatrix} \overline{C}_{nm} \\ \overline{S}_{nm} \end{Bmatrix} = \sqrt{\frac{(n+m)!}{k(2n+1)(n-m)!}}\begin{Bmatrix} C_{nm} \\ S_{nm} \end{Bmatrix} \quad , \qquad k = \begin{cases} 1 \text{ for } m = 0 \\ 2 \text{ for } m \neq 0 \end{cases} \tag{10}$$

The gravity potential W at P can be approximated by the normal potential U and disturbing potential. The disturbing potential T at P is defined as follows:

$$T_p = W_p - U_p \tag{11}$$

The relationship between gravity anomaly and the disturbing potential can be expressed as:

$$\Delta g = -\frac{\partial T}{\partial r} - \frac{2}{r}T \tag{12}$$

Gravity anomaly can be expanded into the following series:

$$\Delta g(r,\theta,\lambda) = \frac{GM_e}{r^2}\sum_{n=1}^{n_{\max}}(n-1)\left(\frac{a_e}{r}\right)^n\sum_{m=0}^{n}[\delta C_{nm}\cos(m\lambda) + \delta S_{nm}\sin(m\lambda)]\overline{P}_{nm}(\cos\theta) \tag{13}$$

where δC_{nm} is the difference of the corresponding coefficients of gravitational potential and normal potential, $\delta S_{nm} = S_{nm}$. Thus, the gravity anomaly of different wavelengths can be computed according to spherical harmonic coefficients (Heiskanen and Moritz 1967).

Since it is not convenient to define the short wave gravity anomaly by spherical harmonic coefficients, we only use the harmonic coefficients of degree 2 - 360 in the calculation of degree anomaly components.

4. GEODYNAMICAL AND GEOLOGICAL ANALYSIS USING HARMONIC SPECTRA AND SATELLITE ALTIMETRY GRAVITY ANOMALY

4.1 Analysis on Gravity Anomaly Spherical Harmonic Components

In this paper, the gravity anomaly from crust difference is estimated and subtracted from the gravity anomaly with the highest resolution obtained from gravity models and satellite altimetry observation, which is defined in this paper as the full degree gravity anomaly. In the so called full degree gravity anomaly, the spectrum components from degree 2 up to degree 360 is from gravity models (degrees 2 - 180 are from GGM02C, 181 - 360 from model EGM9), and for the gravity anomaly degree components higher than 360, we use the residual gravity anomaly in the remove-restore procedure. Then the residual anomaly is compared with anomaly of different degrees to find the best degree range which can express the gravity anomaly from different anomaly source depth in the marginal sea area. In this way, mantle circulation can be analyzed through the different combinations of spectrum components (Sandwell and Smith 2001).

In order to break up the full spectrum of gravity components, we estimated the anomaly contribution of ocean floor topography from the bathymetric model. And then we computed the gravity anomaly degree which can present the gravity anomaly from ocean floor topography so we can remove the ocean floor topography contribution easily from the full spectrum ocean gravity anomaly. In our method, we first compute the gravity anomaly caused by the ocean floor

topography based on the bathymetric model, then compare this gravity anomaly with that from the different degrees of the gravity model to detect the degrees which contribute much to the gravity anomaly caused by the ocean floor topography. The gravity model we used here is EGM96. And the bathymetric model we used is ETOPO2 (http://www.ngdc.noaa.gov/mgg/global/global.html), which is a world DEM dataset with a resolution of 2 minutes, including ocean depths released in 2001 by the National Oceanic and Atmospheric Administration (NOAA).

Two basic principles are applied in this procedure. First, degree components of the gravity anomaly, which undulate consistently with the ocean floor topography, are considered as the contribution of the ocean floor topography. Our method is to calculate and then compare the first derivatives of the degree components of the gravity anomaly along the horizontal directions with those of the ocean floor topography: the consistent components of the gravity anomaly are identified as the anomaly from the ocean floor topography; the inconsistent components are identified as that from the deep crust or mantle. Second, we calculate the sum of the degree anomaly and compare this with the gravity anomaly from the ocean floor topography. The degree group with the least RMS (Root Mean Square) is considered the anomaly of degrees which represent the gravity anomaly from the ocean floor topography. According to this principle, we calculate a series of degree anomaly groups, and compute a 2' × 2' grid value of RMS between the sum of each degree anomaly group and the gravity anomaly from the ocean floor topography. The result is shown in Table 1.

Table 1. RMS differences between gravity anomaly at selected spherical harmonic degrees and topography-derived gravity anomaly.

No.	Gravity Anomaly Degree Groups	RMS/ mGal
1	360, 359	8.21
2	360, 359, 357, 356	8.10
3	360, 359, 357, 356, 352, 351, 350, 346, 345, 344	7.00
4	360, 359, 357, 356, 352, 351, 350, 346, 345, 344, 343, 342, 341, 339, 338, 337, 335	6.39
5	360, 359, 357, 356, 352, 351, 350, 346, 345, 344, 343, 342, 341, 339, 338, 337, 335, 333, 332, 331, 330, 329	6.08
6	360, 359, 357, 356, 352, 351, 350, 346, 345, 344, 343, 342, 341, 339, 338, 337, 335, 333, 332, 331, 330, 329, 328, 327, 326, 324, 323, 321, 320, 318	5.75
7	360, 359, 357, 356, 352, 351, 350, 346, 345, 344, 343, 342, 341, 339, 338, 337, 335, 333, 332, 331, 330, 329, 328, 327, 326, 324, 323, 321, 320, 318, 317, 316, 313	5.31
8	360, 359, 357, 356, 352, 351, 350, 346, 345, 344, 343, 342, 341, 339, 338, 337, 335, 333, 332, 331, 330, 329, 328, 327, 326, 324, 323, 321, 320, 318, 317, 316, 313, 312, 311, 310, 308, 307, 304, 303	4.69
9	360, 359, 357, 356, 352, 351, 350, 346, 345, 344, 343, 342, 341, 339, 338, 337, 335, 333, 332, 331, 330, 329, 328, 327, 326, 324, 323, 321, 320, 318, 317, 316, 313, 312, 311, 310, 308, 307, 304, 303, 302, 300, 299, 297	4.93
10	360, 359, 357, 356, 352, 351, 350, 346, 345, 344, 343, 342, 341, 339, 338, 337, 335, 333, 332, 331, 330, 329, 328, 327, 326, 324, 323, 321, 320, 318, 317, 316, 313, 312, 311, 310, 308, 307, 304, 303, 302, 300, 299, 297, 296, 295, 294, 292	5.59
11	360, 359, 357, 356, 352, 351, 350, 346, 345, 344, 343, 342, 341, 339, 338, 337, 335, 333, 332, 331, 330, 329, 328, 327, 326, 324, 323, 321, 320, 318, 317, 316, 313, 312, 311, 310, 308, 307, 304, 303, 302, 300, 299, 297, 296, 295, 294, 292, 290, 289, 288, 287, 286	6.38
12	360, 359, 357, 356, 352, 351, 350, 346, 345, 344, 343, 342, 341, 339, 338, 337, 335, 333, 332, 331, 330, 329, 328, 327, 326, 324, 323, 321, 320, 318, 317, 316, 313, 312, 311, 310, 308, 307, 304, 303, 302, 300, 299, 297, 296, 295, 294, 292, 290, 289, 288, 287, 286, 285, 283, 282, 280, 279, 277	6.90
13	360 - 318	5.72
14	360 - 313	5.20
15	360 - 303	4.31
16	360 - 297	4.90
17	360 - 292	5.50

As shown in Table 1, group 8 has the least RMS value. So we can deduce the contribution of ocean floor topography to gravity anomaly spectrum in the studied ocean area may be represented by the degrees of group 8. Because the degree anomaly components may not cover all of the gravity anomalies from the ocean floor topography, the least RMS is not 0 mGal. Considering part of the degree components removed according to the first principle, especially those between anomaly degree 303 and 360, may be partly from the ocean floor topography, we calculate the sum of all degree anomalies between degree 303 and 360, and compare this with the result from the ocean floor topography. The RMS is 4.31 mGal, which is better than the result of group 8. As a result, we conclude the gravity anomaly between degree 303 and 360 can represent the gravity anomaly from the ocean floor topography more obviously than degree group 8. However, the gravity anomaly above degree 360 also plays an important part, because the RMS is nearly 5 mGal.

According to the above computation and analysis, in the study area of the China Seas, gravity anomaly from ocean floor topography is equivalent to the gravity anomaly of degree 303 and above. With the geophysical observations on the crustal thickness and density of the crust, we can estimate the gravity anomaly caused by the crust inhomogeneity. Comparing the gravity anomaly of different degree with the gravity anomaly caused by the crust inhomogeneity, we can find useful information about the degree anomaly due to the crust inhomogeneity. The near field and far field effects are equivalent to the gravity anomaly of degree 61 to 303. Residual gravity anomaly after ocean floor topography correction, near and far field correction is equivalent to the full resolution anomaly subtracted the gravity anomaly components above degree 61. The residual anomaly of degree 6 - 60 can be regarded as the gravity anomaly due to the mantle mass inhomogeneity, in which the gravity anomaly of degree 2 - 6 is from the lower mantle; that of degree 7 - 60 is from upper mantle. Considering the gravity anomaly is the difference between the gravity on the geoid and the normal gravity on the ellipsoid, the Bruns correction should be taken to get the so called Bruns anomaly, which can reveal mantle mass distribution better. The flowchart to derive the mantle gravity anomaly from the full gravity anomaly spectrum is shown in Fig. 1.

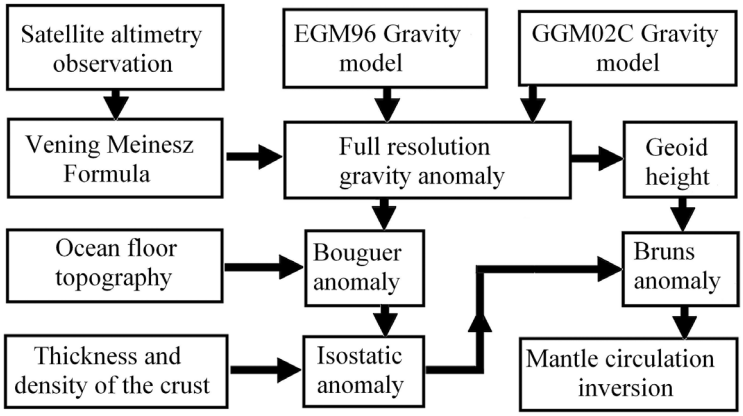

Fig. 1. Flowchart of mantle gravity anomaly derivation.

4.2 Geological Study on the Ocean Floor Topography

According to the analysis in section 4.1, the gravity anomaly between degree 303 and 360 is mainly from the ocean floor topography in the study sea area. However, the RMS of nearly 5 mGal still exists on account of contribution from the gravity anomaly above degree 360.

Gravity anomaly above degree 304 is mainly due to the ocean floor topography (Chang 2006). In order to study the ocean topography in the area of the China Seas in a full scale, we build the gravity anomaly of degree 304 - 360, according to the gravity model EGM96, and compute the gravity anomaly spectrum components above 360 from satellite altimetry observations of Geosat GM and ERS-1 altimetry mission (Fig. 2). Then we get the gravity anomaly components above degree 304, which is used for the geological study on the ocean floor topography of the study sea area.

According to the grid value of the gravity anomaly of the study area in section 2, we compute the gradient of the gravity anomaly and the ocean floor topography along the direction of longitude and latitude. The gravity anomaly is from the grid values we compute above, and the ocean floor topography is from ETOPO2 bathymetric model with resolution of 2 minutes. Thus we can compare the gradient of gravity anomaly and the gradient of ocean floor topography. In our comparison, when the gradient of gravity anomaly and the gradient of ocean floor topography have the same sign, the gravity and the topography are considered to be coincident. According to our computation, the coincidence percentage between the anomaly gravity components above degree 304 and the ocean floor topography is up to 82.4%. However, when only the gravity anomaly of degree 304 - 360 is used in the comparison, the coincidence percentage is only 76.2%; and when only the altimetry derived residual gravity anomaly is used in the comparison, it is 79.8%. Therefore, we can deduce the gravity component above degree 304 accounts for the gravity anomaly from the ocean floor topography best in the study sea area.

4.3 Geodynamical Analysis in Deep Earth

In order to study the geodynamical tectonics in the study area of the China Seas in a full scale, we build the gravity anomaly of degree 2 - 6, 6 - 10, 2 - 10, 7 - 60, and 61 - 303, according to the gravity model EGM96/GG.M02C. The co-

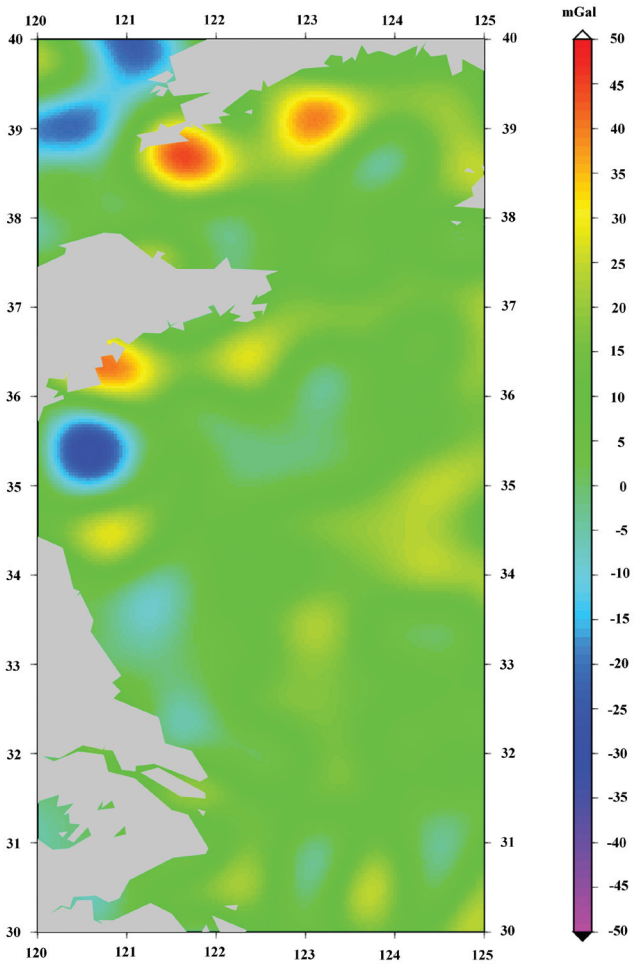

Fig. 2. Gravity anomaly component above degree 360 of the study sea area.

efficients of degree 2 - 180 are from model GGM02C, 181 - 360 from model EGM96. The contours of the components of gravity anomaly are shown in Figs. 3 - 8, in which the unit of the gravity anomaly is mGal, the interval between the contours is 5 mGal.

As shown in Figs. 3 and 5, the isolines of low degree gravity anomaly are all quite sparse and flat, and the absolute anomaly values are quite low. The sparse and flat isolines of the long wavelength components denote the gravity anomaly as being from far away, namely the deep earth, and the low values denote the little transverse difference in density distribution. According to modern geophysical theory, the outer core exists as liquid under high temperature and pressure, so the convection and diffusion and other geophysical phenomena, which can change the redistribution of mass and energy, are fully carried in the core. We can deduce that the low degree gravity anomaly should not come from the core, but from the lower mantle.

According to the seismic wave observation, the velocity of the longitudinal wave is 10.08 - 13.54 km s^{-1} in the lower mantle, and that of the transverse wave is 5.42 - 7.23 km s^{-1} (Chang 2006). With high temperature and pressure, the lower mantle appears to exhibit more plasticity and consequently less rigidity. This means the gravity anomaly from the lower mantle will be at a small level. Comparing Figs. 3, 4, and 5 with each other, we can find anomaly of degree 7 - 10 is dominant in degree 2 - 10. And this can be deduced from the direction of gravity anomaly isolines. So we can deduce that gravity anomaly of degree 2 - 6 in the ocean area (25°N ~ 42°N, 118°E ~ 130°E) is mainly from the lower mantle. The anomaly degree range is basically coincident with the case in the continental area. This shows the mantle below the sea and continent in the eastern part of China could be basically the same.

As a part of the solid lithosphere, rocks of the upper mantle float on half-melted asthenosphere. Under the asthenosphere are solid rocks due to the high pressure and the difference of lithology even though it is at relatively high temperature. The geodynamical performance of the upper mantle is complicated; however, useful information about the mantle circulation can be extracted from the harmonic components of the gravity anomaly. The dynamical imbal-

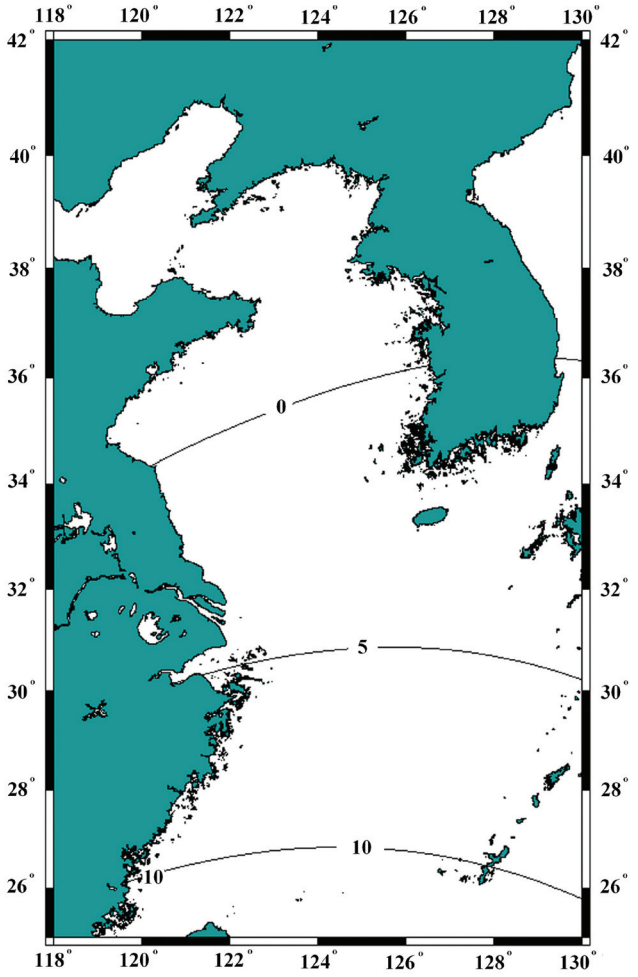

Fig. 3. Gravity anomaly of degree 2 - 6.

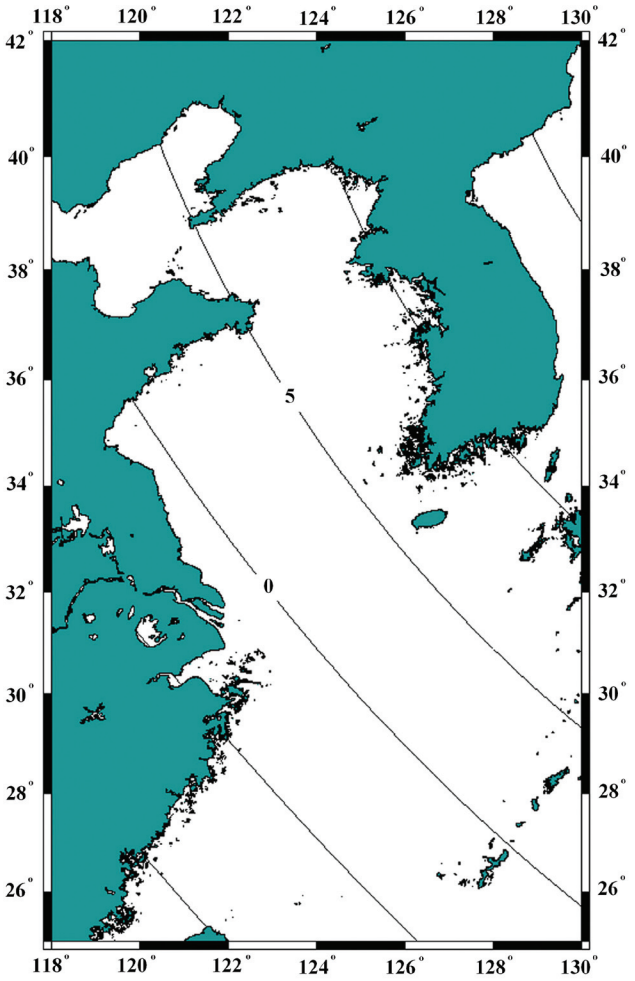

Fig. 4. Gravity anomaly of degree 7 - 10.

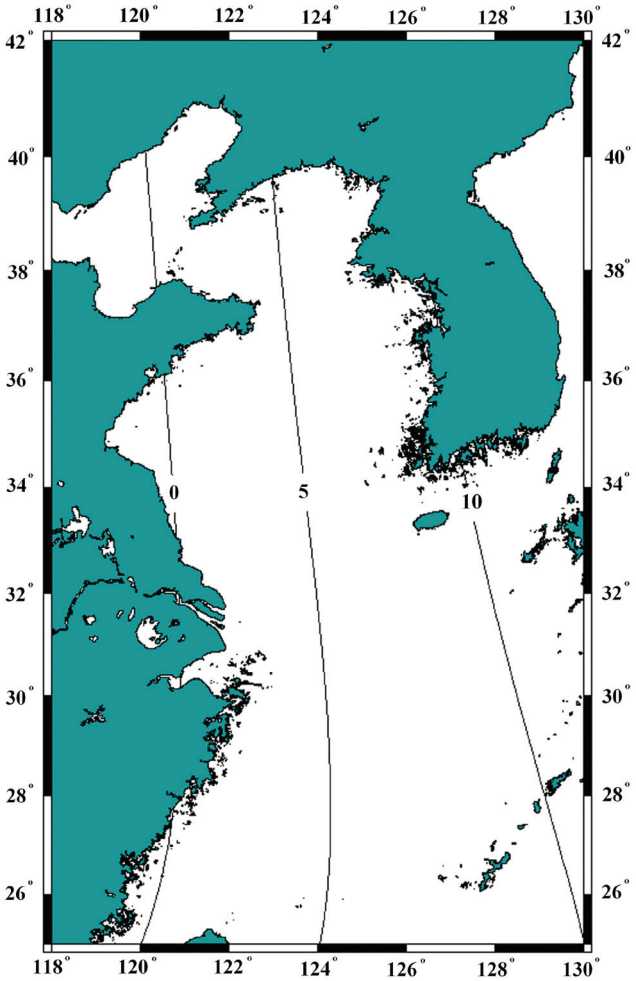

Fig. 5. Gravity anomaly of harmonic degree 2 - 10.

ance of the upper mantle is the most dominant intrinsic factor, which affects the mass and energy exchange between the crust and the upper mantle. Obvious evidence of potential imbalance is the gravity anomaly from the upper mantle being a dominant factor in the structural anomaly of the whole earth. The dynamical imbalance of the upper mantle has been changing the lithosphere by mantle circulation, which is the source of geodynamical movements.

As shown in Fig. 6, when the continental crust below the northwest shallow sea changes into ocean crust below the southeast deep ocean, the gravity anomaly component of degree 7 - 60 changes obviously. The only possible reason is from the upper mantle under the deep crust. It is obvious in Fig. 8 that the value of gravity anomaly increases rapidly at the volcanic island arcs, where the transform between continental block and ocean block occurs. We can deduce from the above that the gravity load from the volcanic island arcs is not fully counteracted by the isostasy of the crust. The density of the lower mantle is a little higher than the norm because the mantle circulation is controlled by the rising flow, and the magma form of the deep earth is of higher density and temperature.

This has already been proved by earlier studies of Hwang et al. (2007). According to their studies, a high gravity anomaly exists in the northern tip of Taiwan due to the high-density mantle from the Tatun and Chilung volcanoes, where very developed terrestrial heat is strong evidence for the very hot rising mantle. The pressure decreases with the temperature when the magma rises, so the density will not change much. It can be deduced that the mantle flow with high density is from the side of deep ocean mantle, so we conclude the rising of the mantle is not the continental mantle flow induced by the density difference but the ocean mantle flow forced by the pressure from the block collision. The rising mantle changes into a volcanic island at the top part when met by cold water, and the lower rising mantle flow is held back to the continental mantle by the hard rock of the volcanic island. High-density magma from the ocean mantle descends because of the lower density of the continental magma (Watts 2001). This process is shown in Fig. 6 as the gravity anomaly decreases at the both sides of the island arc.

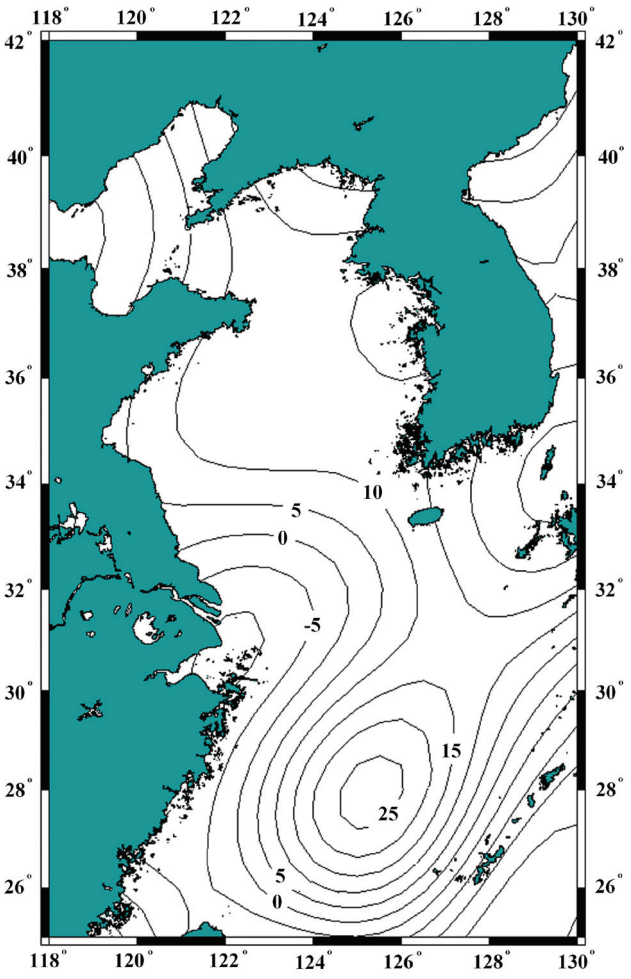

Fig. 6. Gravity anomaly of harmonic degree 7 - 60.

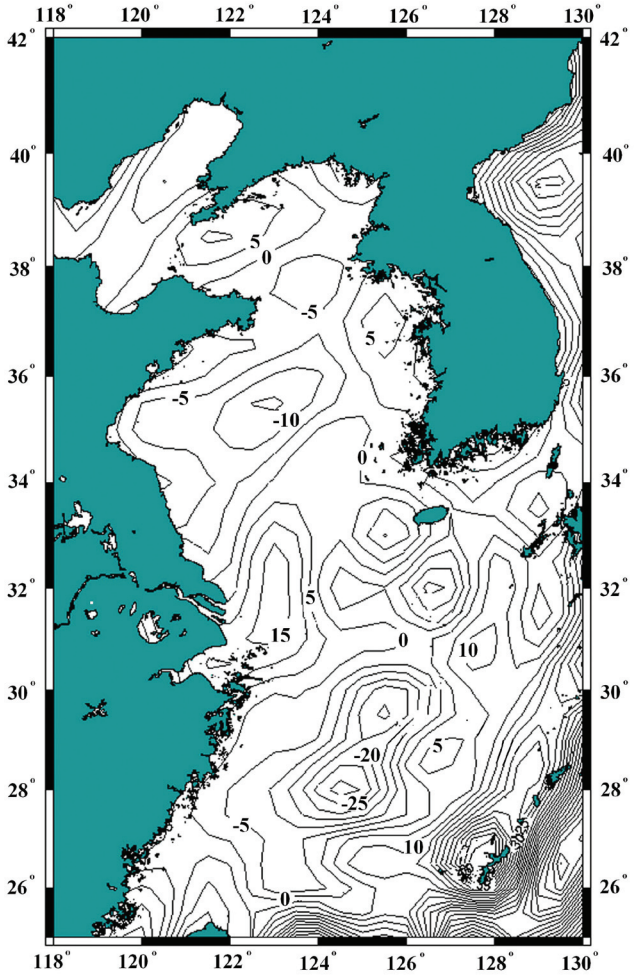

Fig. 7. Gravity anomaly of harmonic degree 61 - 303.

According to the circulation mechanism, the mantle circulation near the island arc is of a small scale, the stress field of which appears as a dispersion belt at the back of the island arc and the trench, and the convergence belt on the island arc. From the island arc to both sides of the arc back and trench, the gravity anomaly component of the upper mantle decreases. The magma from the lower mantle rises to the upper mantle, resulting in violent volcanic activity.

The crust is divided into continental and oceanic crust. The continental crust is thicker and lighter than the oceanic crust (White et al. 1983). This can be seen from the gravity anomaly. As shown in Fig. 7, the gravity anomaly from the crust appears as dense isoline. This shows the isostasy occurs in the crust when the topography changes.

5. SUMMARY

Satellite altimetry provides gravity anomaly over ocean areas, and so can be regarded as an established remote sensing technique with applications in geology and geodynamics. However, there are continuous requests for improvement. Further progress with respect to its application can be reached by increasing spatial and temporal resolution of satellite altimetry. The continuation of current scientific investigation will increase the spectrum and capability of the satellite altimetry-derived gravity anomaly.

In this paper, waveform retracking and innermost zone effects estimation are used to improve the precision of gravity anomaly recovery. The altimetry-derived gravity anomaly and the gravity models, which include the contribution from altimetry, are of interest to both geology and geodynamics. Evidence shows the gravity component above degree 304 accounts for the gravity anomaly from the ocean floor topography best in the study sea area of the China Seas. Gravity anomaly of degree 2 - 6 in the study area of the China Seas is mainly due to lower mantle mass distribution, and the difference between the continent and the ocean is not obvious in the lower mantle. The dynamical imbalance of upper mantle affects the topography isostatic compensation obviously, which is a decisive factor for the crustal movement and hydrostatical balance between the crust and the upper mantle. The gravity anomaly components indicate the

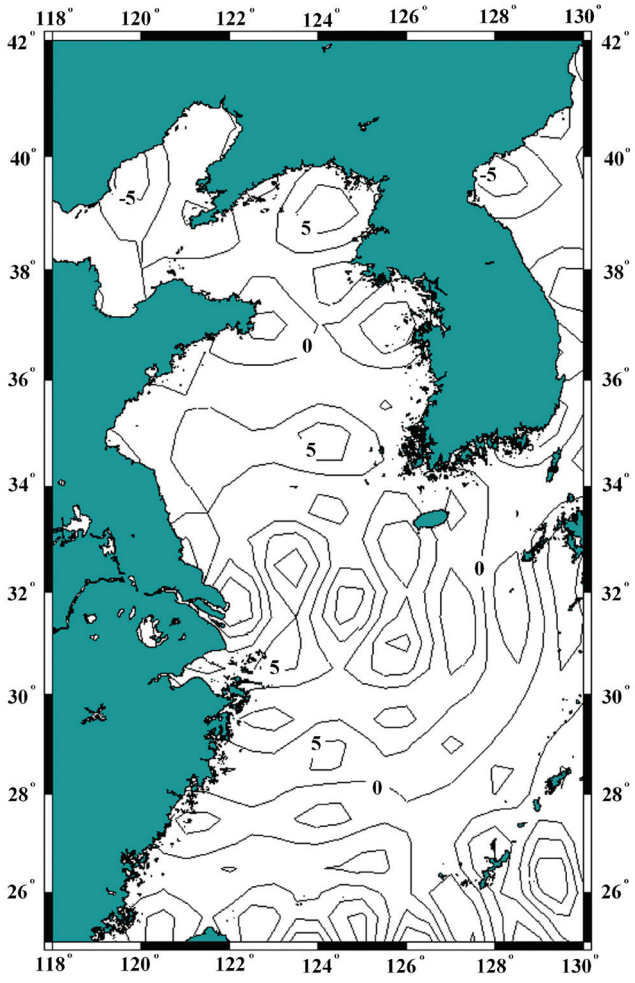

Fig. 8. Gravity anomaly of harmonic degree 304 - 360.

geopotential imbalance from the upper mantle, and the isostatic compensation derived dynamical imbalance may be the source of the global dynamics activity, which changes the lithosphere structure through mantle circulation. Gravity anomaly of degree 7 - 60 in the area of China Seas is mainly due to the mass distribution of the upper mantle. The rising mantle flow with high density is from the deep earth on the ocean side, which dominates the mantle circulation near the volcanic arc. Thus the initial condition of the rising mantle is not induced by the density difference in the continent mantle, but from the plate collision, which makes the ocean mantle rise from the deeper part. The magma from the deep ocean mantle rises to the upper mantle, resulting in violent geodynamic processes, which account for violent volcanic activity near the plate boundary between the ocean and continent.

Acknowledgements This work is supported by the National Natural Science Foundation of China (40474004 and 40774009) and the China national 863 project (2006AA 12Z303). The paper benefits from constructive comments from two anonymous referees.

REFERENCE

Bosch, W., 2004: Geodetic application of satellite altimetry. In: Hwang, C., C. Shum, and J. Li (Eds.), Satellite Altimetry for Geodesy, *Geophys. Oceanogr.*, Springer-Verlag, **126**, 3-21.

Chang, X. T., J. C. Li, and C. Y. Zhang, 2005: Deduction and estimation of innermost zone effects in altimetry gravity algorithm. *Chin. J. Geophys.*, **48**, 1381-1387.

Chang, X. T., 2006: Retracking altimetry waveforms to recover gravity anomaly and its application to geodynamics. Ph. D. Thesis, Wuhan University, Wuhan, China. (in Chinese)

Chang, X. T., J. C. Li, J. Y. Guo, and C. Hwang, 2006: A multi-leading edge and multi-thresshold waveform retracker. *Chin. J. Geophys.*, **49**, 1483-1489.

David, C. M., 1984: Seasat observations of lithosphere flexure seaward of trenches. *J. Geophys. Res*, **89**, 3201-3210.

Dixon, T. H., M. Naraghi, M. K. McNutt, and S. M. Smith, 1983: Bathymetric prediction from Seasat altimeter data. *J. Geophys. Res.*, **88**, 1563-1571.

Guo, J. Y., X. T. Chang, C. Hwang, and Y. T. Liu, 2006: Improved threshold retracker for satellite altimeter waveform retracking over coastal sea. *Prog. Nat. Sci.*, **16**, 732-738.

Haagmans, R., E. de Min, and M. van Gelderen, 1993: Fast evaluation of convolution integrals on the sphere using 1D FFT, and a comparison with existing methods for Stokes' integral. *Manuscr. Geodaet.*, **18**, 227-241.

Heiskanen, W. A., and H. Moritz, 1967: Physical geodesy. Freeman W H and Company, San Francisco, 364 pp.

Hwang, C., 1997: A bathymetric model for the South China Sea from satellite altimetry and depth data. *Mar. Geodesy*, **22**, 37-51.

Hwang, C., 1998: Inverse Vening Meinesz formula and deflection-geoid formula: applications to the predictions of gravity and geoid over the South China Sea. *J. Geodesy*, **72**, 304-312.

Hwang, C., Y. Hsiao, H. Shih, M. Yang, K. Chen, R. Forsberg, and A. V. Olesen, 2007: Geodetic and geophysical results from a Taiwan airborne gravity survey: Data reduction and accuracy assessment. *J. Geophys. Res.*, **112**, B04407.

Sandwell, D. T., 1984: A detailed view of the South Pacific geoid from satellite altimetry. *J. Geophys. Res.*, **89**, 1089-1104.

Sandwell, D. T., and W. H. F. Smith, 2001: Bathymetric estimation. In: Fu, L. L., and A. Cazenave (Eds.), Satellite Altimetry and Earth Sciences, Academic Press, 441-457.

Schwarz, K. P., M. G. Sideris, and R. Forsberg, 1990: The use of FFT techniques in physical geodesy. *Geophys. J. Int.*, **100**, 485-514.

Turcotte, D. L., D. C. Mcadoo, and J. G. Caldwell, 1978: An elastic-perfectly plastic analysis of the bending of the lithosphere at a trench. *Tectonophysics*, **47**, 193-205.

Watts, A. B., 2001: Isostasy and flexure of the lithosphere, Cambridge University Press, Cambridge, 458 pp.

Wessel, P., and W. H. F. Smith, 1995: New version of the Generic Mapping Tools released. *EOS Trans. AGU*, **76**, 329.

Wessel, P., and S. Lyons, 1997: Distribution of large Pacific seamounts from Geosat/ERS-1: Implications for the history of intraplate volcanism. *J. Geophys. Res.*, **102**, 22459-22475.

White, J., R. Sailor, A. Lazarewicz, and A. Le Schack, 1983: Detection of seamount signature in Seasat altimeter data using matched filters. *J. Geophys. Res.*, **88**, 1541-1551.